Evaluation of Dixon based Soft Tissue and Bone Classification in the Pelvis for MR-only-based Radiation Therapy Planning

Michael Helle[1], Nicole Schadewaldt[1], Marloes Frantzen-Steneker[2], Heinrich Schulz[1], Christian Stehning[1], Uulke van der Heide[2], and Steffen Renisch[1]
[1]*Philips Research Laboratories, Hamburg, Germany,* [2]*Department of Radiation Oncology, The Netherlands Cancer Institute, Amsterdam, Netherlands*

INTRODUCTION:

Radiation therapy planning (RTP) and hybrid PET/MR systems can benefit from the superior display of soft tissue contrasts and the delineation of tumor and critical organs in magnetic resonance imaging (MRI). Recently, it was demonstrated that soft tissues as well as cortical bone structures of the pelvic region can be classified with MRI. This was successfully employed for the generation of electron density maps and digitally reconstructed radiographs [1,2]. In this study, an advanced approach on the basis of Dixon MR techniques with subsequent reconstruction workflow is introduced for soft tissue and bone classification. For the first time, this method is evaluated in patients with corresponding CT data and radiation therapy plans. Dose calculations based on the MR generated simulated CTs are compared to the true CT based dose.

MATERIALS and METHODS:

The data of six patients scheduled for pelvic radiation therapy were acquired during clinical routine measurements on a Philips 3.0T Achieva TX System using the body coil for transmission, and a 6-element phased-array coil for signal reception. T1-Dixon imaging parameters were as follows: 3D Cartesian fast-field echo acquisition, TE_1/TE_2 = 1.1ms/2.1ms, TR = 3.3ms, α = 10°, 1.7x1.7x2.5mm^3 voxel size, 300x400x350 mm^3 FOV, and 1:49min imaging time. Bone-enhanced images were generated by automatically thresholding the low-intensity regions of the Dixon in-phase image with subsequent background removal. Bowel content misclassified as bone was reduced by filtering with a rigidly registered probabilistic bone atlas. Water (soft tissue fractions) and fat tissue (adipose tissue fractions) were derived from a conventional Dixon reconstruction of the nearly in-phase (TE_2) and out-phase images (TE_1). In addition, bone marrow is estimated from adipose tissue by the application of a probabilistic marrow atlas. Probabilistic atlas data was generated beforehand from a database of computed tomography images [3]. Simulated CT maps were generated by encoding the classified voxels with population average Hounsfield values of soft tissue (52 HU), adipose tissue (-75 HU), air (-968 HU), marrow (417 HU) and cortical bone (1188 HU) and combining them into one image.

In order to distinguish between the effects of geometric misclassification and variability in individual density values, "stratified CTs" were generated in which all voxels within typical density ranges for air (-1000 to -210 HU), adipose tissue (-209 to -20 HU), muscle/connective tissue (-19 to 200 HU), bone marrow (201 to 900 HU) and cortical bone (901 to 2000 HU) were replaced with the same values as listed above. All MR derived simulated CT maps were evaluated against corresponding stratified true CT images by volumetric and voxelwise comparison of the individual tissue classes. Radiation treatment planning was performed in Pinnacle v9.6. Finally, dose calculation based on true CT data was compared to dose calculation on MR generated simulated CTs.

RESULTS:

Figure 1 shows a representative slice of a simulated CT of one patient compared to the corresponding stratified true CT. The volumetric comparison of MR derived simulated CT maps and stratified true CT images show a reasonably similar number of bone and air voxels, however, the simulated CTs present more fat classified voxels and less water content as compared to the true CT (fig. 2). Table 1 shows that more than 90% of voxels classified as air in the simulated CT maps are also classified as air in the stratified true CT images. For water tissue, this holds for almost 87%, whereas for voxels classified as fat only about 59% are within the same tissue class of the corresponding stratified true CT. For bone structures (marrow + cortical bone) only 44% present the same classification in the stratified true CT images; a significantly larger amount of about 50% of bone structures of the MR derived simulated CT are classified as water tissue in the stratified true CT images. Radiation dose computed on MR derived simulated CTs and stratified true CT images demonstrates good agreement in the qualitative comparison of isodose lines in the treatment plans (fig. 3). A quantitative analysis of mean target dose calculations based on each of the modalities presents differences ranging from 0.3% to 1.6% (mean 0.7%).

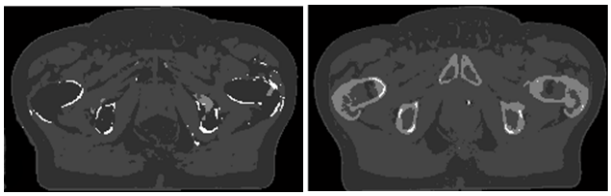

Figure 1: Example slice of one patient of a MR derived simulated CT (left) and corresponding stratified true CT (right) with tissue classified as air, fat, water, bone marrow, and cortical bone fractions.

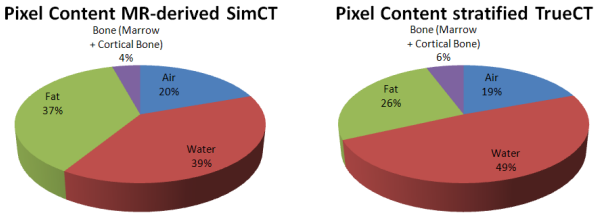

Figure 2: Volumetric comparison averaged over all patients of the individual tissue classes in MR derived simulated CT and stratified true CT.

SimCT \ TrueCT	Air (%)	Water (%)	Fat (%)	Bone (%) (marrow+cortical)
Air (%)	90.8 ± 3.0	2.9 ± 0.5	6.4 ± 2.7	0.0 ± 0.0
Water (%)	2.8 ± 1.2	86.7 ± 1.6	7.2 ± 1.5	3.2 ± 0.6
Fat (%)	1.3 ± 0.8	32.9 ± 5.8	58.7 ± 6.2	7.1 ± 1.4
Bone (%) (marrow+cortical)	0.2 ± 0.2	50.4 ± 4.5	6.1 ± 2.5	43.4 ± 5.1

Table 1: Voxelwise comparison of the individual tissue classes averaged over all patients in MR derived simulated CT and stratified true CT after rigid registration.

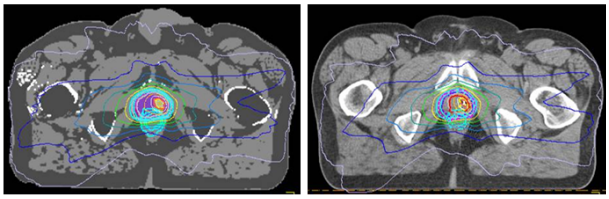

Figure 3: Comparison of radiation dose computed on MR derived simulated CT (left) and stratified true CT (right). The isodose lines correspond well between both dose calculations.

DISCUSSION and CONCLUSION:

The advanced Cartesian T1-Dixon technique in conjunction with subsequent image processing allowed for tissue classification in the pelvis in order to generate simulated CT maps and to perform radiation therapy dose calculation. The larger number of water voxels in the stratified true CT images when compared to the MR derived simulated CTs can be mainly attributed to different bladder filling as CT was always made after MRI. The higher amount of fat classified voxels in the MR derived simulated CTs probably refers to misclassified marrow tissue. Bone marrow basically consists of spongy bone structures and fat content. However, the applied T1-Dixon method only allows measuring signal of the latter whereas no signal of spongy bone can be acquired. Therefore, an additional probabilistic marrow atlas is employed to prevent marrow voxels being misclassified as fat. On the contrary, in CT images, bone marrow density is represented from both fat and spongy bone tissues and presents an averaged density of both tissue types.

Such effects also contribute to differences in a voxelwise comparison as shown in table 1. Different body outlines contribute to differences in a voxelwise comparison as well and might be due to the receive coil placed on the patient during MR measurements. However, some kind of supporting device that allows to position the receive coil as close as possible to the patient without distorting the body contour might solve this problem.

In addition, imperfect registration of MR and CT images has a high impact on the outcome of voxelwise comparision, especially for small structures like cortical bone. Cortical bone structures are only represented as layers of one or two pixel thickness so that small registration errors will result in large errors in overlap measures. However, this is rather a limitation of the comparison methodology than of the approach itself. Consequently, for this analysis, bony structures were compared as a whole (marrow + cortical bone).

In conclusion, taking into account five tissue classes for the generation of MR based simulated CTs results in acceptable differences of mean target dose when compared to respective computations using true CT data.

REFERENCES:

1. Helle M et al, ISMRM 2013, #768; 2. Schadewaldt N et al, ASTRO 2013, #3423; 3. Vik T et al, IEEE ISBI 2012, p: 338-341